the ANALYST

THE VOICE OF THE WATER TREATMENT INDUSTRY

Stabilization of the Magnetite Layer in Steam Boilers With Tannins

Louis Godbout (TGWT, Inc.); Axel Gambou-Bosca, Ph.D. (Centre de métallurgie du Québec); and Christian Fowelin, Ph.D. (Korn GmbH)

Abstract

After having been the treatment of choice for boiler corrosion and scale control for more than a century, the use of tannins decreased in the 20th century in favor of cheaper, but often underperforming synthetic products. Resurgence in their use is now underway because of the energy and water savings they allow and other environmental benefits of green chemistry. Until recently, the empirically proven benefits of tannins were not understood scientifically. This is largely because their complex chemistry and structures have only been tackled in the past decade. The physico-chemical reactions occurring in the boilers are also finally becoming clearer. It was recently demonstrated that tannins adsorb on various metal surfaces. We have now further advanced our understanding of how this adsorption affects the development of the passivation layer of steel in boiler conditions.

At high pH, temperature, and pressure, steel coupons rapidly develop a strikingly different appearance in the presence of tannins. Typically, the surface is visibly smoother and more adherent, with noticeably less spalling of magnetite than in control samples. We have studied the microstructure of these passivation layers using scanning electron microscopy coupled with energy dispersive spectroscopy (SEM/EDS) as well as grazing incidence X-ray diffraction (GI-XRD). Their corrosion behavior was studied by potentiodynamic polarization and electrochemical impedance spectroscopy (EIS). The differences in thickness, porosity, adherence, crystal composition, and structure are in line with improved performances. These characteristics also explain why the use of tannins rapidly brings down to a minimum the evolution of hydrogen in boiler steam: a denser and less porous passivation layer becomes stable as it limits the Schikorr reaction at the underlying metal surfaces.

How Magnetite Films Form

The study of films with reduced reactivity that protect an underlying metal from corrosion started in the 18th century (1), and then sparked the interest of Michael Faraday in the 1830s. The term "passivity" was coined by Faraday's friend and collaborator, Christian Schönbein, in 1836. Together they quickly

understood that passivation involved the creation of a protective layer of metal oxide on the surface of the steel (2). This "bluing" or "blackening" of steel could be obtained either by heating, or by chemical or electro-chemical treatment. It was and remains important in manufacturing and can be seen in many objects used in everyday life, such as screws, bolts, springs, and all sorts of tools.

Passivation remained a subject of great interest for many chemists through the 19th century. Great strides were made in the 20th century, especially with the develop-ment of electrochemical instrumentation (3). To this day, scientists have used the newest techniques to investigate the structure and formation of oxides and hydroxides that form on iron or steel. These will vary according to the conditions under which they form, but it is magne-tite (Fe_3O_4) or, more precisely $Fe^{II}Fe^{III}_2O_4$ (i.e., ferrous-ferric oxide) that coats the surfaces of well-operated steel boilers and passivates them.

Magnetite was one of the first substances whose crys-talline structure was determined by X-ray diffraction by W.H. Bragg, the founder of crystallography himself, in 1915 (4) (Figure 1).

The reaction (Equation 1) that produces magnetite was first described by Schikorr in 1933 (7):

$$3\,Fe + 4\,H_2O \rightarrow Fe_3O_4 + 4\,H_2 \hspace{2cm} Eq.\ 1$$

(N.B. This equation shows the reaction of iron and water to produce magnetite, but in fact Schikorr only described the transformation of iron hydroxide to magnetite:
$3\,Fe(OH)_2\ ---\ [150\ °C] \rightarrow Fe_3O_4 + 2\,H_2O + H_2)$

However, the simplicity of this overall reaction hides many other reactions and mechanisms that are vastly more complex but also more revealing of exactly how magnetite forms under different conditions of pH, temperature, pressure, and ionic conditions.

Here is one series of proposed steps (Reactions 1-6) that may explain why it is favored in the boiler (8, 9).

1. $Fe^0 \leftrightarrow Fe^{2+} + 2e-$ $E_O = 0.44$ V   Reaction 1
2. $Fe^{2+} + 6\,H_2O \rightarrow [Fe(H_2O)_6]^{2+}$ Reaction 2
3. $[Fe(H_2O)^6]^{2+} \leftrightarrow Fe(OH)_2 + 2H^+ + 4\,H_2O$ Reaction 3
4. $2\,Fe^{II}(OH)_2 + 2\,H_2O \rightarrow 2\,Fe^{III}(OH)_3 + H_2$ Reaction 4
5. $n\,Fe^{III}(OH)_3 \rightarrow [Fe^{III}O(OH)]n + n\,H_2O$ Reaction 5
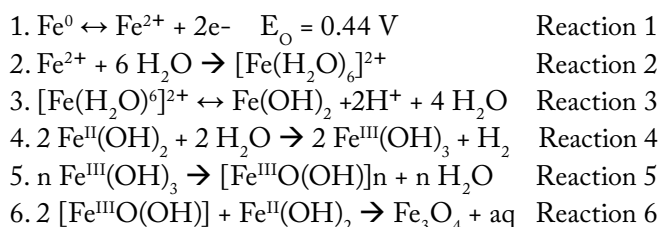6. $2\,[Fe^{III}O(OH)] + Fe^{II}(OH)_2 \rightarrow Fe_3O_4 + aq$ Reaction 6

Figure 1: (Left) An X-ray diffraction pattern of a magnetite crystal growing epitaxially from a steel surface. (Right) the crystal structure of magnetite. The black spheres are Fe^{3+}, the green spheres are Fe^{2+}, and the red spheres are O^{2-}. As Bragg described it in 1915, "The divalent atom lies at the centre of a tetrahedron of oxygen atoms, and the trivalent at the centre of an octahedron" (4). (Note: Figure 1 images are from References 5 and 6.)
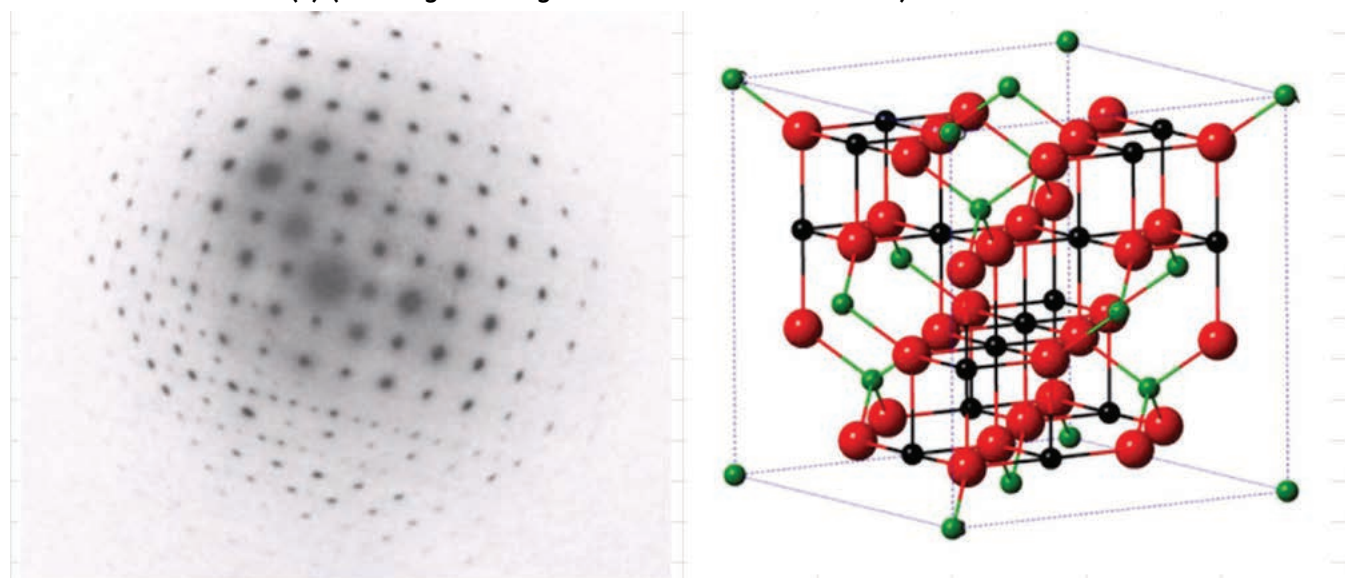
At high pH, Reaction 3 would be favored, while Reaction 4 would proceed only at high temperatures such as are found in boilers. However, as we will see, things are much more complicated, as different reactions occur at different locations in the structures of passive layers as they grow.

These can be single or multi-layered, more or less adhesive to the underlying steel, more or less porous, and hence, may confer different degrees of protection from corrosion. The magnetite formation rate will vary according to how these structures evolve. It would be desirable that this rate rapidly diminish to a minimum after a thin and dense layer of oxide is formed and prevents further oxidation, but this is rarely the case. In fact, under certain circumstances, oxidation of iron to magnetite can be an important source of metal loss if the layer is too porous and continuously spalls. Another source of worry with an undiminishing high rate of the Schikorr reaction is the production of hydrogen, which will readily diffuse through steel and embrittle it as it reacts with carbon to form methane. In fact, the monitoring of hydrogen in steam is recommended for high-pressure systems (10).

Since the late 1950s, many researchers have attempted to understand and categorize the various morphologies of the magnetite layers. The pioneers were Bloom, Potter, Mann, Castle, Field, Friggen, Holmes, Marsh, and Moore, who produced magnetite passivation layers in autoclaves under controlled conditions (6, 11–21). They characterized them by microscopy and by measuring the rate at which the layer was produced, either by monitoring the evolution of hydrogen or by measuring the weight gained as magnetite formed on the surfaces. Two major morphologies were described and came to be known as "Bloom films," which consist of a single thin layer of large crystals, and "Potter-Mann films," which consist of two thick layers—an underlying one of small compacted crystals and a top one of large and loosely bound crystals with well-defined spinel structure (see Figure 2).

Much effort was invested in understanding how two such dissimilar structures could form under very similar conditions. In both experiments, steel samples with clean surfaces were oxidized at high temperature and pressure in caustic solutions. The only difference was that the Bloom films were produced in sealed steel capsules of relatively small volume, whereas the Potter-Mann films were produced in mild-steel pressure vessels of large volume, the interior of which was already covered with magnetite.

For more than a decade, clever experiments were designed to understand how the different structures arose. It was determined that the Potter-Mann films formed because the fresh iron surfaces were in galvanic contact with magnetite previously formed on the insides of the autoclaves that acted as a cathode. More interestingly, it was determined that hydrogen concentration also affected the outcome. This is because hydrogen gas does not diffuse as easily through magnetite as it does through steel, whereas hydrogen ions do, leading to gradients and different reaction equilibria through the layer. This was to prove of great importance in understanding the mechanisms involved in the formation of multilayered films.

These are more interesting, as they are the type seen in industrial systems, as opposed to "Bloom films," which are seen only in controlled lab experiments. But how exactly they are formed was the subject of another four decades of research and is still ongoing.

Figure 2: (Left) A very thin, 5- to 10-micron (µm), single-layered "Bloom film" made of large crystals fused to the surface. (Right) A very thick, 40- to 50-µm, double-layered "Potter-Mann film" with a compact underlying layer of small crystals and a loose top layer of large, well-formed crystals. (Figure 2 is from Reference 19.)

Understanding the reason for the small-grain morphology of the base layer came early. As iron is oxidized to magnetite, its volume increases about by a factor of 2.1 (the Pilling-Bedworth ratio); it is thus inevitable that stresses will be created that could fracture the crystals (22). The work of Moore and Jones (6), who followed the transformation of oriented crystals (emerging epitaxially from iron grains) into small randomly oriented crystals, demonstrated this convincingly. A thorough explanation of how the grains are reduced to their comminution limit by a cracking mechanism because of the compressive stresses was later given by Robertson and Manning (23). This cracking necessarily involves the creation of micro- or perhaps nano-pores, which are necessary to explain how a second layer develops.

Understanding the reason for the larger, well-defined crystals found in the top layer may also seem obvious. It can only develop if there is iron transport from the oxide layer, as Castle and Mann believed (17), or from the underlying surface metal, as later models propose. The iron must remain in a soluble form as it moves through pores along grain boundaries in the base polycrystalline layer. Once it reaches the surface, it can be oxidized to magnetite that can grow unconstrained, from small

nuclei to very large crystals. The difficulty, however, was to elucidate why the pores remain unclogged, as one would expect that any iron in solution would precipitate to fill and block them. Two mechanisms to explain this were offered by Bignold, et al. (24), and by Bergé, et al. (25). The latter convincingly suggests that higher hydrogen levels at the metal-oxide surface and in the pores will reduce magnetite to a soluble hydroxide that can then migrate to the surface to be oxidized again and deposit on the larger magnetite crystals.

Figure 3 presents cartoons of some of the models suggested over the years, showing what reactions occur and, more importantly, where. Refinements of these models that agree more closely with the measurements of reaction rates and the location of hydrogen evolution are still being proposed (9, 22). In parallel, even though the conditions are drastically different than in a boiler, studies of the structure of passivation films produced electrochemically (3, 26, 27) and spectroscopic studies that can detect the presence of various other iron oxides, such as the crystallographically close maghemite (28, 29) and hydroxides, may reveal more about what precisely happens in the formation of a magnetite film.

Figure 3: Various models proposed to explain the formation of the double-layered "Potter-Mann film" passivation layer. Clockwise from top left are Castle and Mann (17), Tomlinson (30), Cheng and Steward (31), and Shibata (32). The last two, as well as that of Bornak's (33), are variants of Tomlinson's model. That of Robertson (not presented here) is also noteworthy for its detailed unravelling of what reactions occur where in the structure, but it is not represented here graphically (22).
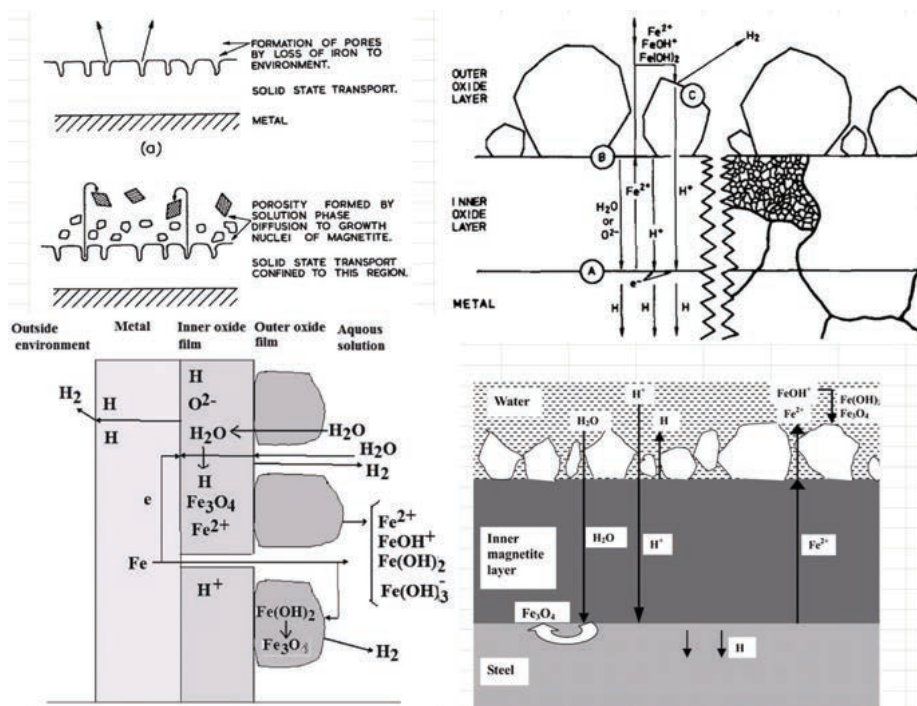
"The most striking observations are the traces of blistering and spalling on the untreated coupons oxidized without tannins."

Unfortunately, many of the studies on the formation of magnetite films are limited to systems in which only sodium hydroxide (NaOH) or lithium hydroxide (LiOH) are present in pure water. A few have explored the effect of various metal chlorides, which seem to have a very negative effect, leading to the formation of multi-layered, nonprotective passivation layers (16). Others have explored the effect of complexing agents and water treatment chemicals on the morphology and resistance of the passivation layer (34–39).

In this study, we propose to evaluate the effect of tannin-based corrosion inhibitors on the magnetite layer, through experiments done in synthetic boiler water that is more realistic than the simple solutions heretofore used.

Materials and Methods

"Synthetic" boiler water was prepared using the following recipe (all reagent-grade chemicals were from Sigma-Aldrich):

> 320 milligrams (mg) of anhydrous sodium carbonate (Na_2CO_3)

> 320 mg of anhydrous sodium sulfate (Na_2SO_4)

> 500 mg of sodium chloride (NaCl)

> 4 milliliter (mL) of 1 M NaOH solution

The recipe was completed with reverse osmosis (RO) water to a volume of 1,000 mL.

For each experiment, 50 mL of this solution was placed in a 100 mL Teflon® container designed to fit into a stainless-steel autoclave with a screw system to keep the contents sealed at high temperatures. After placing the autoclave in a glovebox, argon was used to displace any air and was bubbled through the solution for 30 minutes. Using a micropipette, 100 microliters (μL) of one of a tannin solution[A] was added. A C1010 steel coupon (either polished or unpolished) was placed inside, and the Teflon® cover secured. The metal cap of the autoclave was then screwed tightly before placing it in an oven at 180 °C for 96 hours.

Grazing incidence X-ray diffraction (GI-XRD) was done using a Bruker model D8 Advance instrument. The X-ray source was copper (Cu) (1.5418Å) with a 40 kilovolt (kV) voltage and a 40-milliamp (mA) current. The angle of incidence (2θ) was 3°. The primary source passed through a Göbel mirror (deflection of 0.876°) et axial Soller slits (2.5°) before hitting the sample. The secondary rays diffracted by the sample pass through Soller slits (0.2°), a nickel filter (0.02-millimeter (mm) thick), et axial Soller slits (2.5°) before hitting the detector. The diffractograms were acquired from 25° to 75°, in 0.02° increments and a 1-second integration time.

Potentiodynamic polarization and electrochemical impedance spectroscopy (EIS) were performed in 3.5% NaCl solutions in a K0235 flat cell from London Scientific Limited using a Princeton Applied Research/AMETEK VersaSTAT 4 potentiostat/galvanostat with a frequency response analyzer (FRA).

Scanning electron microscopy (SEM) was performed using a JEOL JSM7600F instrument with a field-effect electron gun (FEG). Energy dispersive spectroscopy X-ray analysis (EDS) was performed with an Oxford Instrument detector and software.

Results and Discussion

General Visual Appearance of Coupons and Spalling of Magnetite

Figure 4 shows unpolished coupons produced in four different experimental conditions. The polished coupons show similar features. The most striking observations are the traces of blistering and spalling on the untreated coupons oxidized without tannins. This is indicative of a weakly adherent magnetite layer. The blistering seems to have progressed through successive detachments, as shown by the "worming" path and shape of the traces. Similar zones were seen on both polished and unpolished coupons but give only a qualitative estimate of the quantity of loosely bound magnetite, more abundantly found at the bottom of the autoclave, as shown in Figure 5.
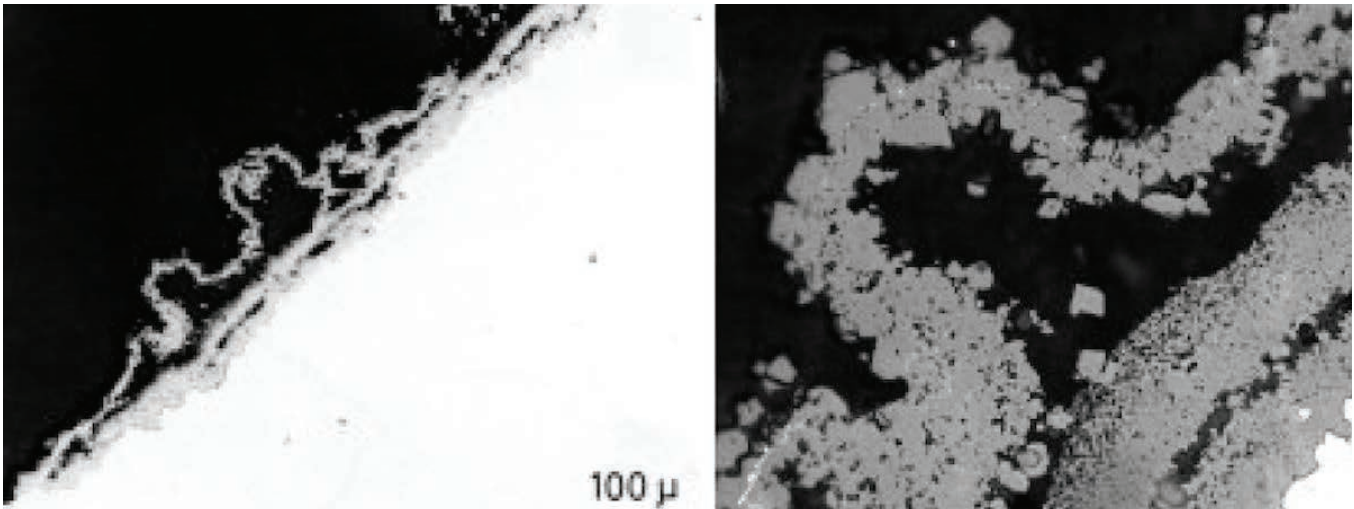
Figure 4: (Left to right) Unpolished mild steel coupons—untreated, TG3304, TG3124, and TG3106 treatments. The colors observed give an indication of the thickness of the films (40).

Figure 5: Detached magnetite at the bottom of the reaction vessel of the autoclave.

Figure 6: Undulating oxide detaching from a surface. (Images from Reference 41.)

In Potter and Mann's experiments, up to half of the magnetite produced would fall away from the sample surfaces, but there is no indication that this happened by blistering (16). We have already mentioned that the Pilling-Bedworth ratio of magnetite (i.e., the ratio of the volume of the elementary cell of a magnetite to the volume of the elementary cell of iron) is 2.1 and that it is posited that the stresses that this volume expansion creates explain the random polycrystalline underlayer of Potter-Mann films. Could the compressive strain also explain the blisters? Huijbregts and Snel certainly showed this to be the case in a solution containing 0.1 M nickel chloride (NiCl) (see Figure 6) (41), but our own microscopic observations suggest an added mechanism, as will be seen below.

Finally, the darker and duller appearance of the magnetite on the untreated coupon is indicative of a thicker layer of magnetite with a rough, light-dispersing surface. In the case of the tannin-treated coupons, the layer is smooth and shiny, and sometimes so thin as to create a bluish interference color. In the case of TG3124 treatment, it is so thin that it leaves visible some the sheen of the underlying metal.

GI-XRD

As can be seen in Figure 7, GI-XRD allows us to identify the crystalline species present. In all cases, only the signature peaks of iron and magnetite were seen, but it is possible that small amounts of maghemite (γ-Fe_2O_3) are also present, as its peaks fall very close to those of magnetite. Traces of maghemite have been found in

boiler systems before (28) but would be inconsequential for our analysis.

As can be seen in Figure 8, GI-XRD also allows for the determination of an average crystallite size by applying the Scherrer equation (Equation 2) to the largest magnetite peak. Equation 2 can be written as:

$$\tau = K\lambda/\beta\cos\theta \qquad\qquad \text{Eq. 2}$$

Where:

τ = The mean size of the ordered (crystalline) domains, which may be smaller or equal to the grain size.

K = A dimensionless shape factor, with a value close to unity. The shape factor has a typical value of about 0.9, but varies with the actual shape of the crystallite.

λ = The X-ray wavelength.

β = The line broadening at half the maximum intensity (FWHM), after subtracting the instrumental line broadening, in radians. This quantity is also sometimes denoted as $\Delta(2\theta)$.

θ = The Bragg angle.

The average size of the tannin-treated sample is roughly half that of the untreated, a very significant difference if one considers that porosity of a compacted layer of small crystals will be much less than that of large crystals.

Figure 7: The top diffractogram is taken on an untreated coupon oxidized in deoxygenated synthetic boiler water. The bottom one is taken on a coupon treated with TG3124 in deoxygenated synthetic boiler water. In both, only the peak characteristic of iron and magnetite can be seen. This is also the case for the diffractograms taken on TG3304 and TG3106 treated coupons. Notice that the peaks for the TG3124 are broader and shorter, indicating a smaller average crystal size.
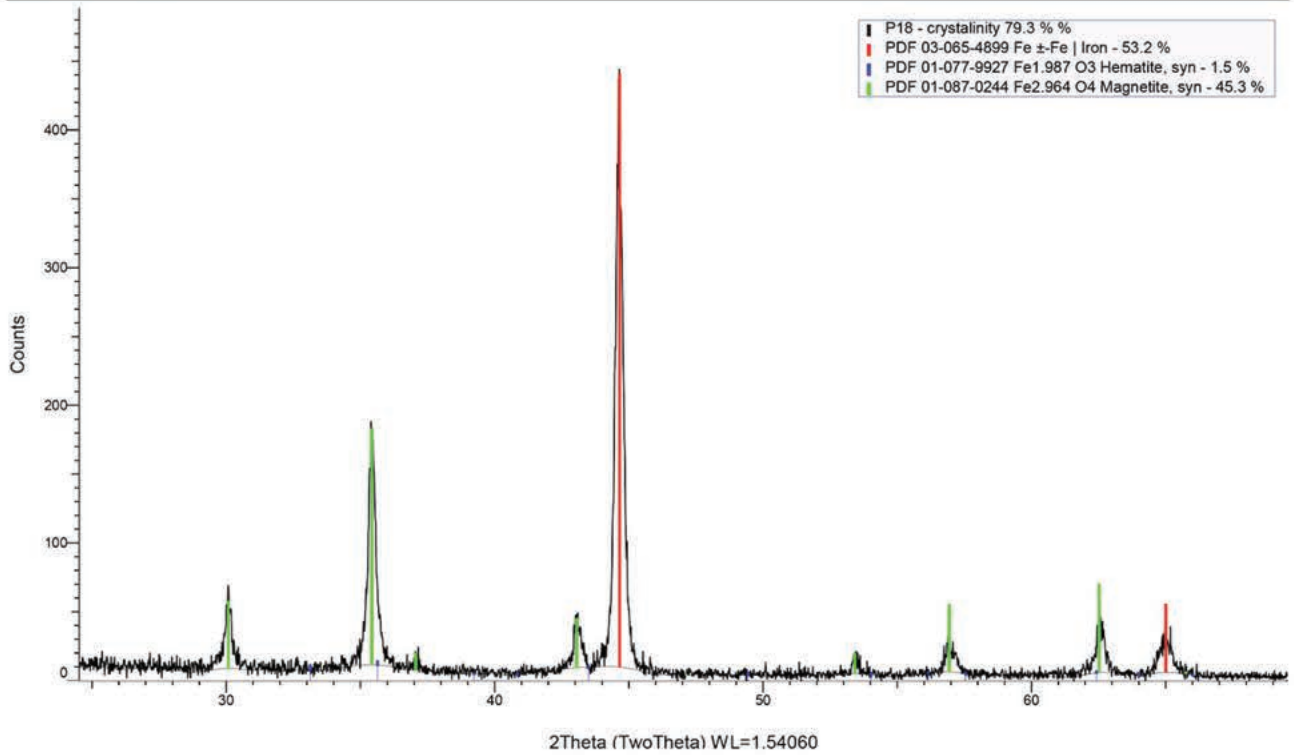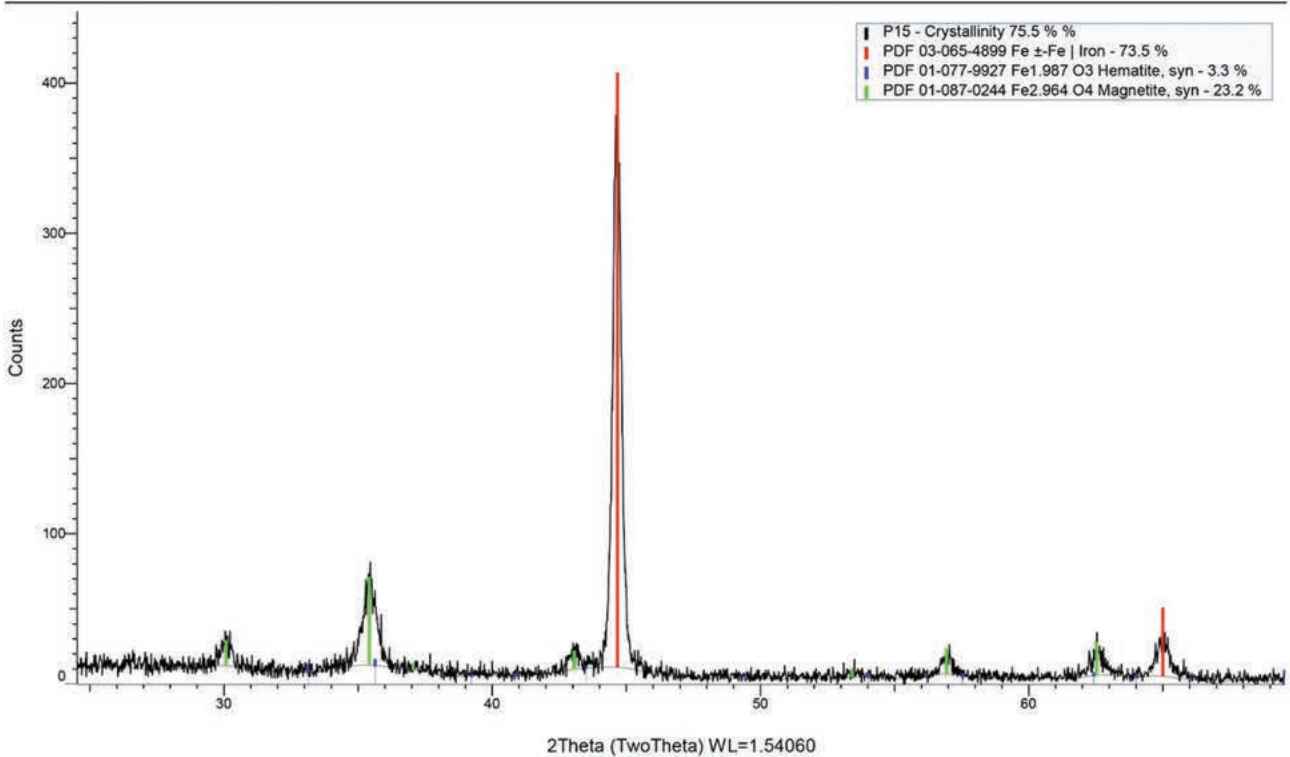
Figure 8: The top diffractogram, showing only the main magnetite peak, is taken on a coupon without treatment oxidized in deoxygenated synthetic boiler water, while the bottom one is from a coupon treated with TGWT 3124. The Scherrer equation allows us to extract the average size of the magnetite crystals: 31.17 nanometer (nm) for the untreated coupon, and 15.24 nm for the TG3124. These are the extremes seen in our experiments. TG3304 and TG3106 have intermediate sizes of 28.09 nm and 21.89 nm, respectively.
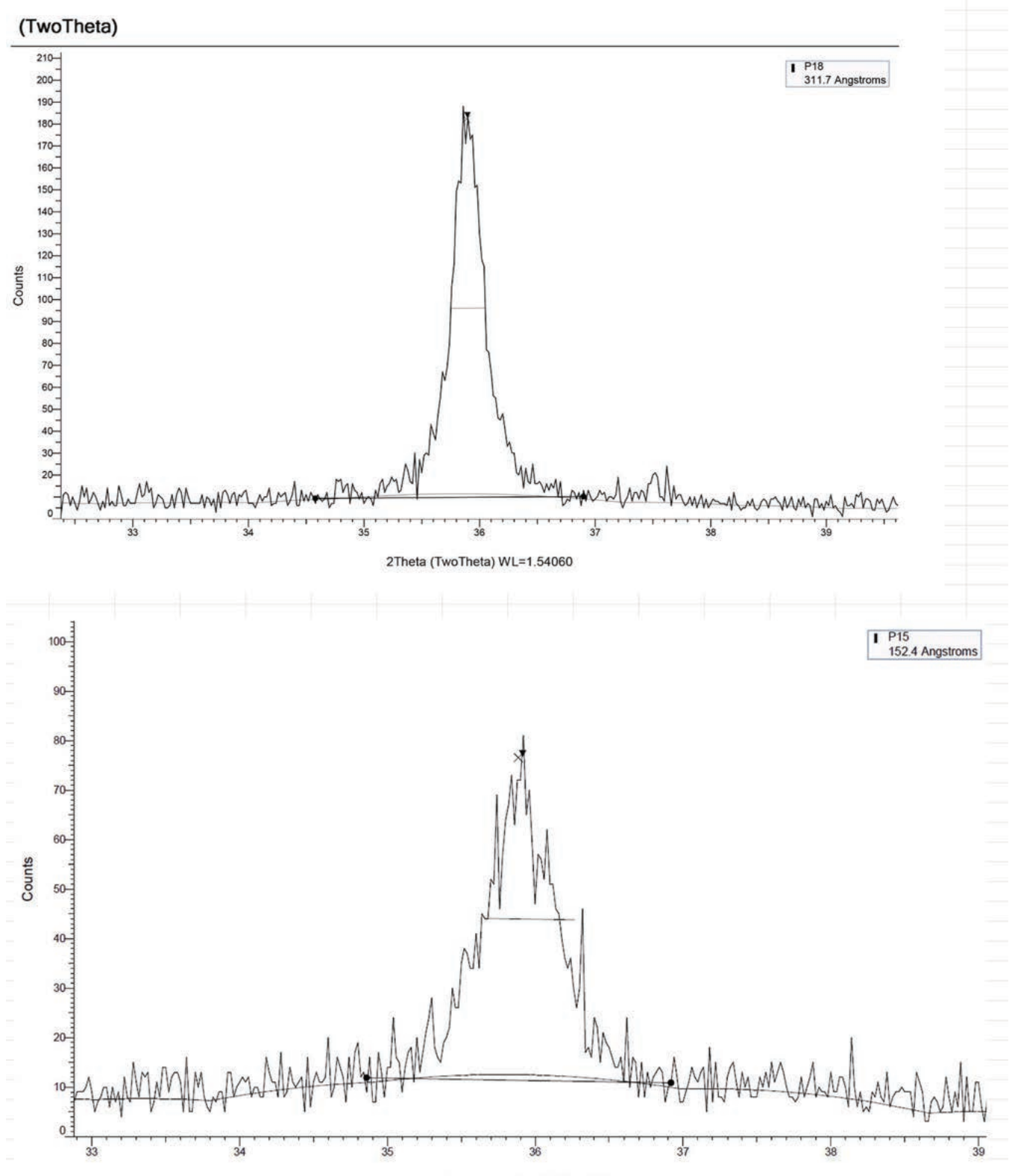
SEM and EDS

SEM reveals much more than just an average crystal size. It shows clearly and unsurprisingly that for the untreated sample, we have a Potter-Mann film, with large, well-formed crystals sitting mostly on top of a layer of smaller particles, having no clear crystalline morphology, as shown in the two images on the left in Figure 9. What is most surprising is the fact that for the tannin-treated sample, seen on the right in Figure 9, there is a complete absence of large-sized crystals on a much smoother surface. There are fewer defects, suggesting that the passivation layer is less porous and has stabilized enough to prevent further egress of iron from the metal surface to the surface of the oxide. Moreover, it can be seen in the untreated sample that small,well-formed crystals are lodged in cracks. Any growth of these is likely to disrupt the magnetite layer and participate in the process of blistering and spalling without having to create a large undulating structure.

Figure 9: (Left) The untreated coupon at medium and high magnifications. Notice the well-formed crystals lodged in cracks. Any growth of these will disrupt the magnetite layer. (Right) A tannin-treated coupon at the same magnifications. No large crystals are to be seen, which is an indication that there is no iron transport from the underlying metal to the surface.
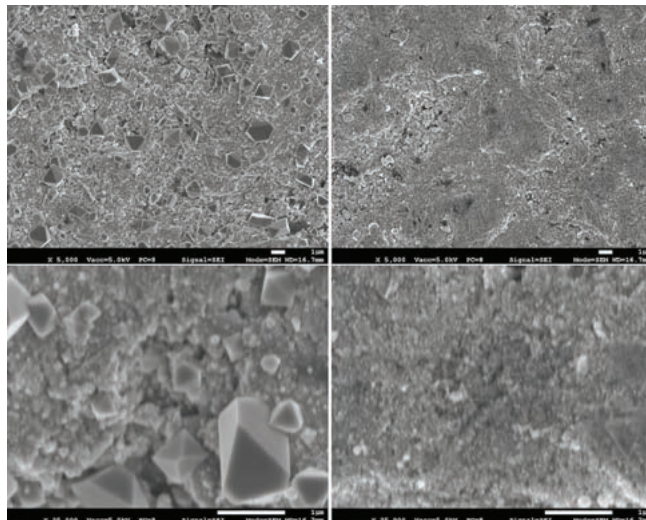
> ## "SEM reveals much more than just an average crystal size."

A further interesting observation on the untreated sample can be obtained by backscattered SEM imaging and EDS analysis of the blistered and unblistered zone. The image of the blistered zone appears darker, an indication of a smaller proportion of heavy elements, in this case iron. The measurements of the oxygen content yield the same unexpected result. There is more oxygen on the blistered zone when we would have expected less than in the magnetite-covered zone (see Figure 10). It would appear that the iron in the blistered zone has already undergone a first step in its oxidation back to magnetite, perhaps to maghemite, or more likely to hydroxides. This would support the mechanism of oxidation proposed by Carvalho and Kelly, shown in Figure 11 (9). Other spectroscopic techniques could confirm this hypothesis.

Figure 10: The backscattered electron image at the top shows the border between the magnetite-covered region (left) and the blistered area (right). The elemental composition in the spectra below show 12.8% oxygen in the magnetite zone and 21.9% in the blistered zone, an unexpected result.
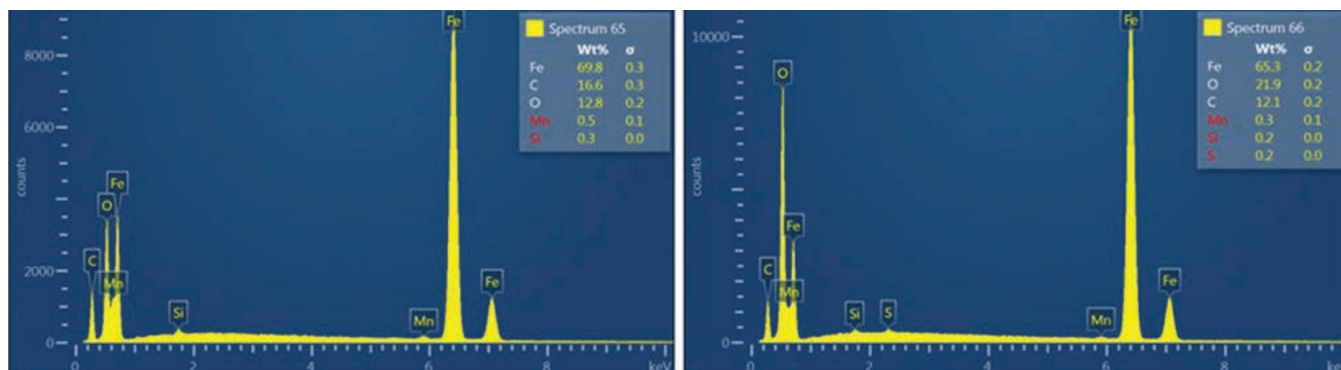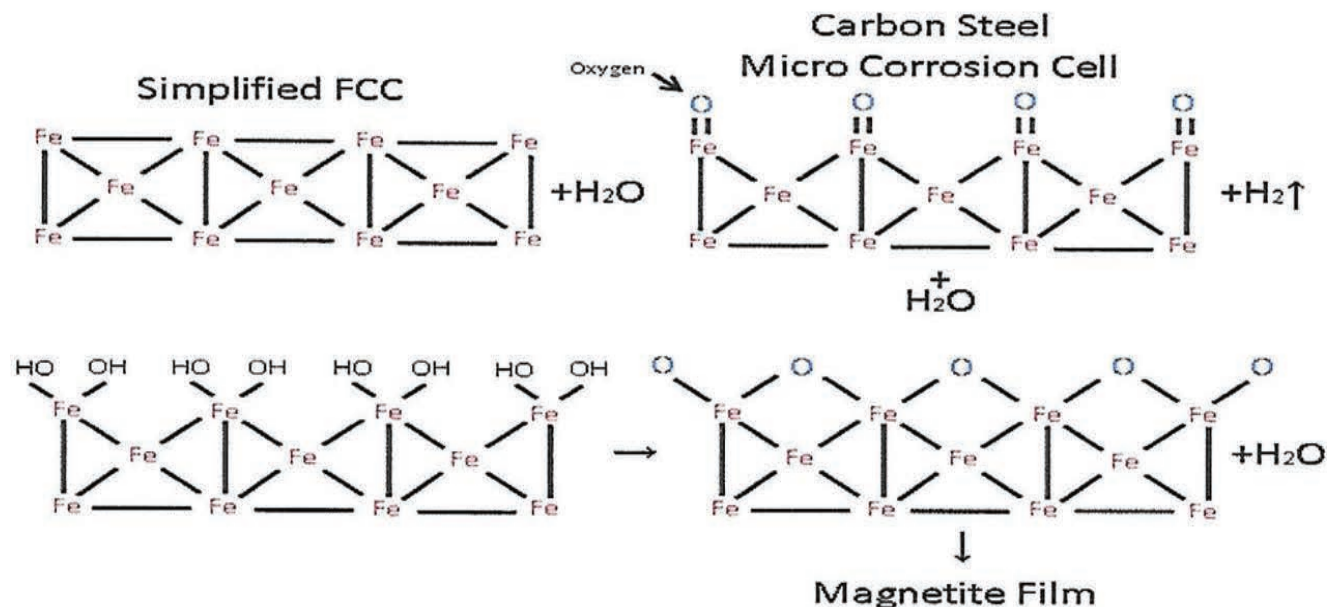
Figure 11: Carvalho and Kelly's suggested mechanism for the initial stages of magnetite film formation (9). The formation of hydroxides might explain the high percentage of oxygen seen by EDS in the blistered zone that resembles the bare metal surface.

Electrochemistry

The experimental conditions for our measurements were extremely harsh, using 3.5% NaCl solutions. The results deal with worst-case scenarios for which steel parts would never be submitted, but are useful in comparing the passivation layers obtained by different treatments:

Rest 1 hour (h) at open circuit potential (Eocp), which is close to the corrosion potential of the substrate. Potentiodynamic polarization from -25 millivolt (mV) to 1.5 volt (V) versus Eocp.

Electrochemical impedance spectroscopy was used to investigate the ability of a tannin/magnetite layer to slow down the corrosion rate of the underlying steel substrate:

Potentiostatic EIS after 1h OCP from 100 kilohertz (kHz) to 10 megahertz (mHz), Ac 10 mV

Figure 12 is useful in understanding what information can be gained from potentiodynamic measurements. Figure 13 shows the results for our experiments, namely a marked decrease in corrosion intensity for the TG3124 sample. In analyzing these results, it is good to keep in mind that the passivation layer for the tannin-treated sample is much thinner than the very thick but porous layer of the untreated sample.

Figure 12: Typical information gained from potentiodynamic curves.
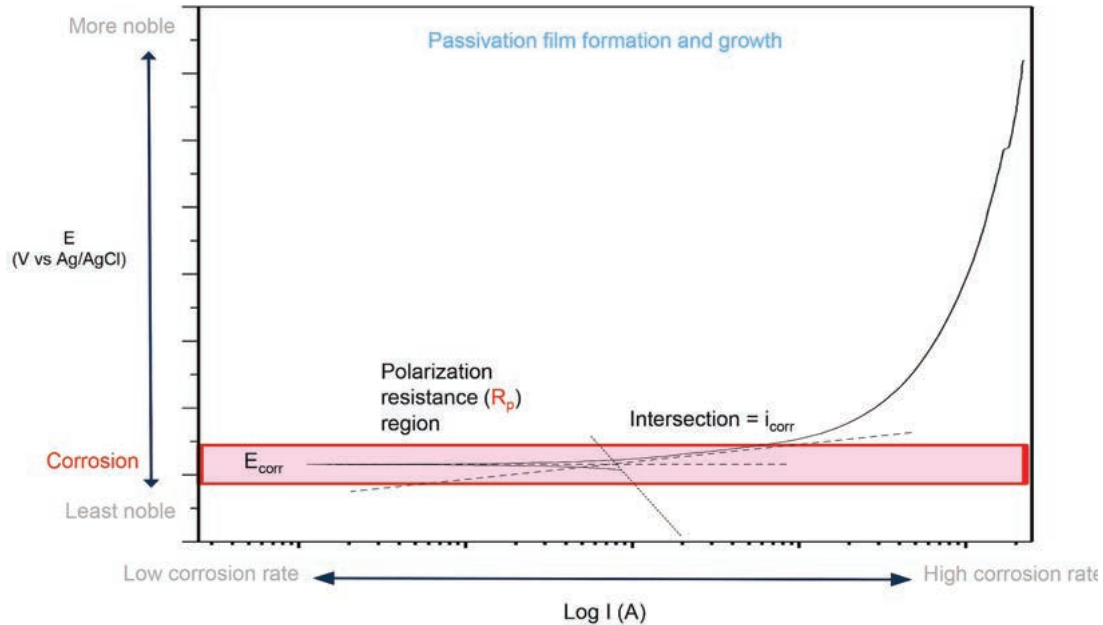
"The gradual increment of the impedance value in the tannin-treated samples suggests the formation of a protective passive oxide film on the steel surface."

Figure 13: Typical potentiodynamic curves for the bare metal sample as-received, the untreated oxidized sample, and two tannin-treated samples. The arrow indicates a decrease in corrosion intensity (corrosion current).
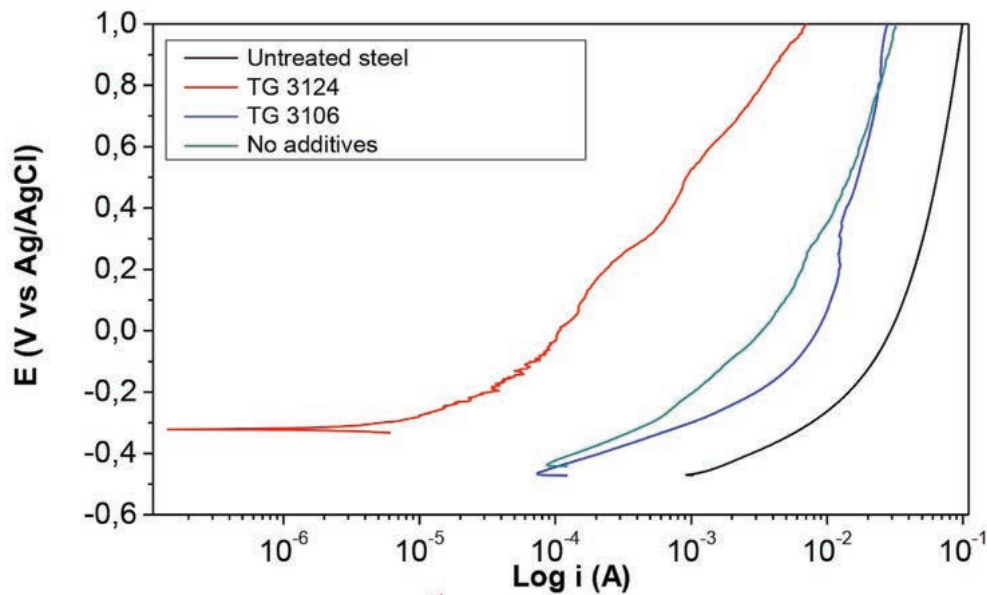

Figure 14 shows typical impedance-frequency Bode plots: the impedance at the lowest studied frequency (0.01 Hz) varies with the treatment. The gradual increment of the impedance value in the tannin-treated samples suggests the formation of a protective passive oxide film on the steel surface.

Figure 14: Impedance-frequency Bode plots for the bare metal sample as-received, the untreated oxidized sample, and two tannin-treated samples.
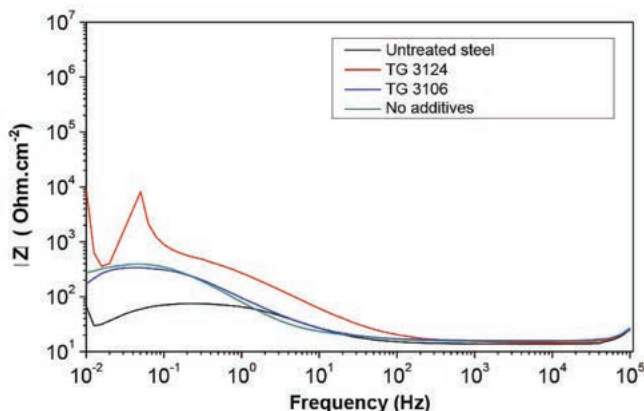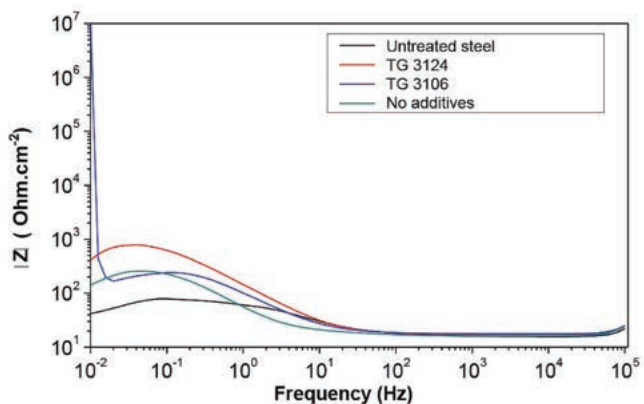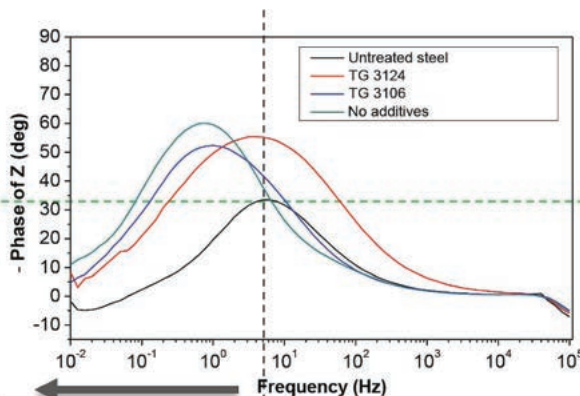

Figure 15: Frequency-phase Bode plots for the bare metal sample as-received, the untreated oxidized sample, and two tannin-treated samples.
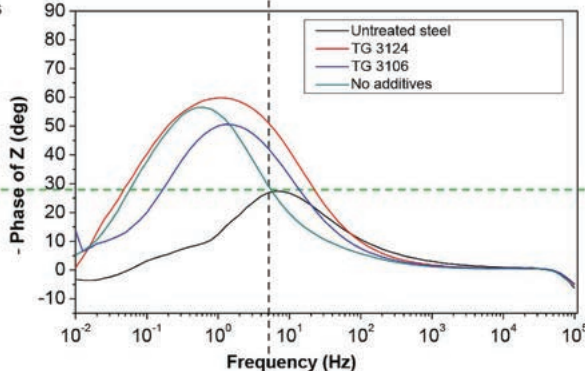

Finally, Figure 15 shows frequency-phase Bode plots. The maximum phase angle for all four materials in service environment exposure is between 50° and 60°, respectively, and lesser for the base metal. Also, the maximum angle value is shifted toward lower frequencies (5 Hz for as-received material, and between 1 Hz to 0.3 Hz for tested samples). The shifting of the phase angle at the lower frequency is attributed to the formation of double-layer capacitance and the reduction in the anodic surface area of substrate. This phenomenon indicates that the surface was covered with protective and thick passive layers. Finally, the high frequency values of the phase for bare, TG3124, TG3106, and unprotected metal show that the system behaves like a pure resistance being the electrolyte resistance. This, combined with the low-|Z| value for the same high frequency, demonstrates that the saltwater solution comes in contact with the metal.

Hydrogen Evolution in Tannin-Treated Boilers

Although we did not monitor the amount of hydrogen produced in our experiments, the larger amount of magnetite (both adhered and spalled) on the untreated sample indicates that this byproduct of the Schikorr reaction was more abundant. The thinner layers of magnetite on the tannin-treated samples indicates either an overall lower rate of the reaction throughout the 96-hour experiments, or, more likely, a reduced rate after a certain thickness of a denser, less porous magnetite film is formed in the presence of tannins.

Supporting this hypothesis is data from an industrial boiler shown in Figure 16. Soon after the water treatment is switched from a conventional one to tannins, the level of hydrogen in the steam drops, indicating that tannins reduce the rate of the Schikorr reaction.

Figure 16: Hydrogen measurements in the steam of a boiler before and after initiating a tannin-based treatment at the time indicated by the red arrow.
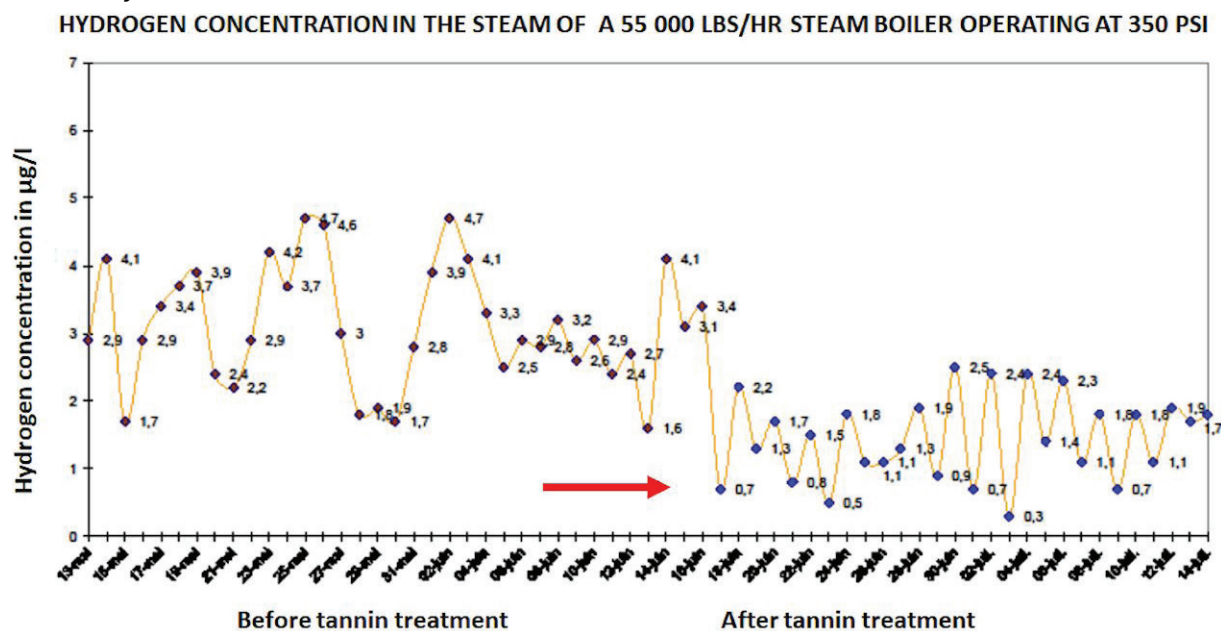
Concluding Remarks and Further Work

Recent understanding of the mechanism by which tannins protect mild steel boiler surfaces came from the work of Dargahi, et al. (42, 43), who showed, by measurements in a quartz-crystal microbalance with dissipation (QCM-D), that tannins adsorb on mild steel (see Figure 17). Electrochemical impedance spectroscopy measurements showing improved corrosion resistance supported the hypothesis that an iron-tannate film was the source of the passivation. Though this may be the case for closed loops, it is unlikely that the same situation applies to boilers in which magnetite is always found on the surfaces.

Figure 17: Adsorption isotherm for a tannin-based inhibitor onto mild steel at pH 10.5 and room temperature. Circles represent the experimental data, while the solid line represents the corresponding value from the Langmuir isotherm. Inset: experimental data (circles) show an excellent correlation with the linearized Langmuir isotherm (from Reference 43).
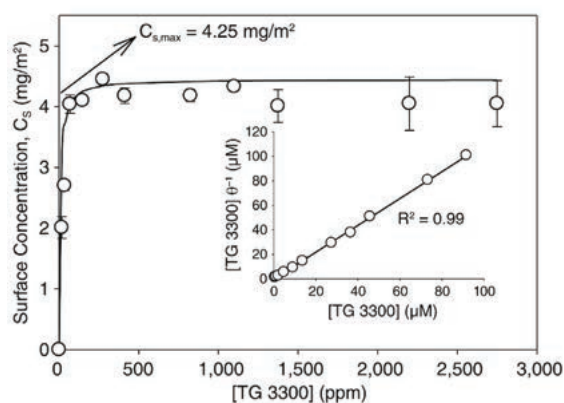
The data presented in this article suggests that we have another phenomenon at work that allows us to present an alternate model to explain the effect of tannins in boilers (see Figure 18). Adsorption of tannins on steel does not prevent an underlying magnetite film from forming but affects its structure by *stabilizing* it in the following ways:

1. A single layer of magnetite is produced with a reduced thickness.
2. The crystal size in this layer is greatly diminished, as also is the porosity.
3. Spalling and blistering are eliminated, indicative of an improved adhesiveness to the metal.
4. Migration of iron from the base layer of metal is stopped.
5. Hydrogen production is reduced.
6. Resistance to corrosion is improved.

Further work will hopefully reveal the mechanism by which this happens, but in view of the likely models by which magnetite is produced (outlined in our introduction), the most probable hypothesis is that pore-blocking plays a critical role. Key questions to be answered are:

1. Does this happen only at the surface, or throughout the porous magnetite structure as it evolves?
2. Does it occur by adsorption or by precipitation of iron-tannate complexes inside the pores?

The answers to these questions would help to explain the process and role that tannins play.

Figure 18: (Top) A cartoon representing the previous model to explain the improved corrosion resistance when tannins are used. (Bottom) A cartoon representing the stabilization of the magnetite layer by tannins to explain the improved corrosion resistance.
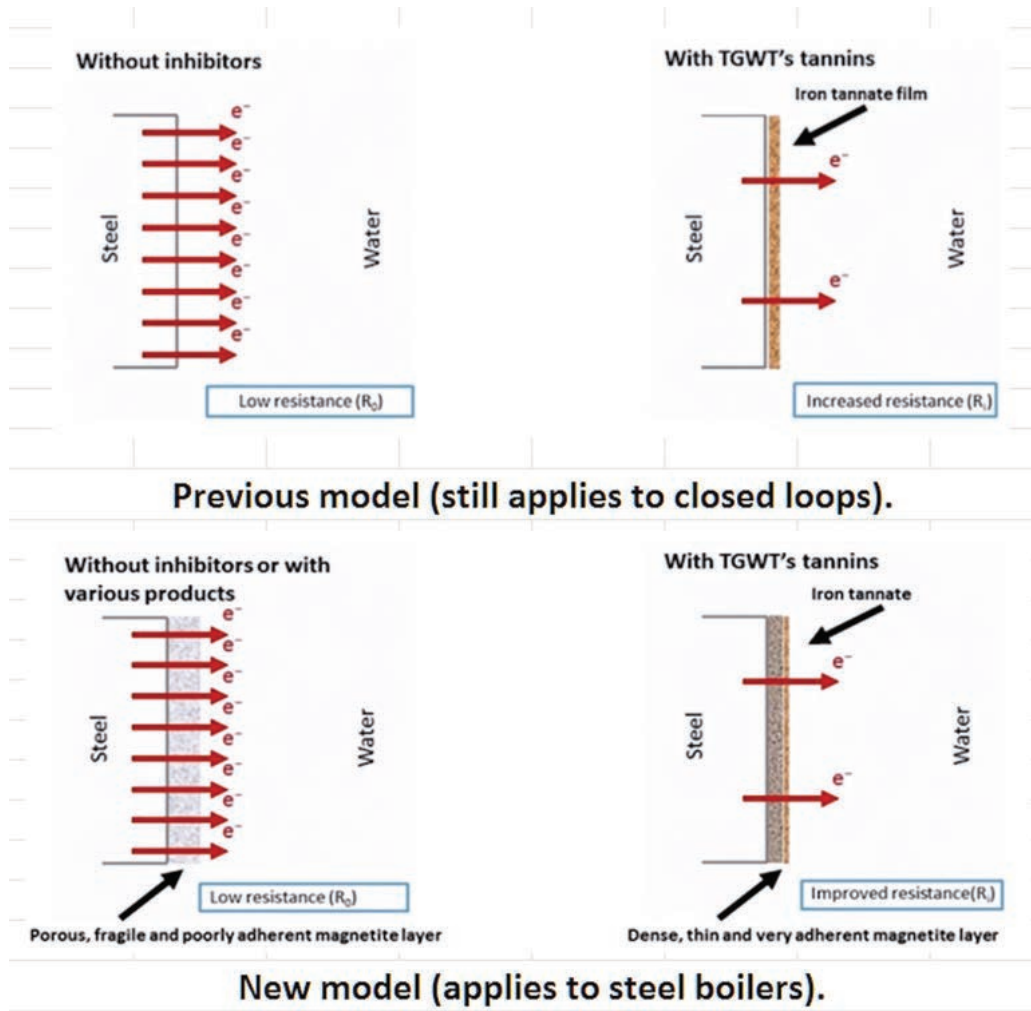
Acknowledgements

References

1. Keir, J. (1790). "Experiments and observations on the dissolution of metals in acids, and their precipitations; with an account of a new compound acid menstruum, useful in some technical operations of parting metals," Philosophical Transactions of the Royal Society of London, 1790(80): pp. 359-384.

2. Schönbein, C.F.; Faraday, M. (June 17, 1836). "On a Peculiar Voltaic Condition of Iron," Richard Taylor, Lion Red Court, Fleet Street.

3. Davenport, A.J.; Oblonsky, L.J.; Ryan, M.P.; Toney, M.F. (2000). "The Structure of the Passive Film that Forms on Iron in Aqueous Environments," *Journal of the Electrochemical Society 147(6),* pp. 2162-2173.

4. Bragg, W. (1915). "The Structure of Magnetite and the Spinels," *Nature 95(2386),* p. 561.

5. Wu, W.; Wu, Z.; Yu, T.; Jiang, C.; Kim, W.S. (2015). "Recent Progress on Magnetic Iron Oxide Nanoparticles: Synthesis, Surface Functional Strategies and Biomedical Applications," *Science and Technology of Advanced Materials 16(2),* p. 023501.

6. Moore, J.B.; Jones, R.L. (1968). "Growth Characteristics of Iron Oxide Films Generated in Dilute Lithium Hydroxide Solution at 300°C," *Journal of The Electrochemical Society 115(6),* pp. 576-583.

7. Schikorr, G. (1933). "Über Eisen (II)-hydroxyd und ein ferromagnetisches Eisen (III) hydroxyd," *Zeitschrift für anorganische und allgemeine Chemie 212(1)* ("About Iron (II) Hydroxide and a Ferromagnetic Iron (III) Hydroxide," *Journal of Inorganic and General Chemistry),* pp. 33-39.

8. Noack, M. (April 17-21, 1989). "Oxygen Scavengers," presentation at Corrosion '89, New Orleans, LA. New Orleans, LA.

9. Carvalho, L.; Kelly, J.A. (March 6-30, 2016). "The Chemistry and Crystallographic Characteristics of Passive Magnetite Film Formation," presented at Corrosion 2016, Vancouver, B.C., Canada.

10. Roubaty, J. (1986). "La corrosion des chaudières; son suivi par l'analyse de l'hydrogène dans la vapeur," *La Technique modern 78(1-2)* ("Corrosion of Boilers; Followed by the Analysis of Hydrogen in Vapor," *Modern Technology 78(1-2)),* pp. 17-20.

11. Bloom, M.; Krulfeld, M. (1957). "A Hydrogen Effusion Method for the Determination of Corrosion Rates in Aqueous Systems at Elevated Temperature and Pressure," *Journal of the Electrochemical Society 104(5),* pp. 264-269.

12. Potter, E. (1961). "Oxidation of Mild Steel in High-Temperature Aqueous Systems," *Proceedings of the 1st International Congress on Metallic Corrosion,* London, UK, pp. 417-426.

13. Potter, E. (1963). "Mechanism of Magnetite Growth on Low-Carbon Steel in Steam and Aqueous Solutions up to 550°C," in *Proceedings of the 2nd International Congress on Metallic Corrosion,* Houston, TX.

14. Potter, E. (1962). *The First International Congress on Metallic Corrosion, 1961,* Butterworths, London, 712 pages, Pergamon.

15. Bloom, M.; Newport, G.; Fraser, W. (1964). "Steel Corrosion Mechanisms: The Growth and Breakdown of Protective Films in High-Temperature Aqueous Systems at 316°C," *Journal of The Electrochemical Society 111(12),* pp. 1343-1347.

16. Potter, E.; Mann, G. (1965). "The Fast Linear Growth of Magnetite on Mild Steel in High-Temperature Aqueous Conditions," *British Corrosion Journal 1(1),* pp. 26-35.

17. Castle, J.; Mann, G. (1966). "The Mechanism of Formation of a Porous Oxide Film on Steel," *Corrosion Science 6(6),* pp. 253-262.

18. Castle, J.; Masterson, H. (1966). "The Role of Diffusion in the Oxidation of Mild Steel in High-Temperature Aqueous Solutions," *Corrosion Science 6(3-4),* pp. 93-104.

19. Marsh, T. (1966). "The Morphology of Magnetite Growth on Mild Steel in Alkaline Solutions at 316°C," *Journal of the Electrochemical Society 113(4),* pp. 313-318.

20. Field, E.M.; Holmes, D. (1965). "Nucleation and Growth of Magnetite Films on Pure Iron in High-Temperature Water," *Corrosion Science 5(5),* pp. 361-370.

21. Friggens, H.A.; Holmes, D. (1968) "Nucleation and Growth of Magnetite Films on Fe in High-Temperature Water," *Corrosion Science 8(12),* pp. 871-881.

22. Robertson, J., (1989) "The Mechanism of High-Temperature Aqueous Corrosion of Steel," *Corrosion Science 29(11-12),* pp. 1275-1291.

23. Robertson, J.; Manning, M. (1988). "Criteria for Formation of Single Layer, Duplex, and Breakaway Scales on Steels," *Materials Science and Technology 4(12),* pp. 1064-1071.

24. Bignold, G.; Garnsey, R.; Mann, G. (1972) "High-Temperature Aqueous Corrosion of Iron Development of Theories of Equilibrium Solution Phase Transport through a Porous Oxide," *Corrosion Science 12(4),* pp. 325-332.

25. Berge, P.; Ribon, C.; Paul, P.S. (1977). "Effect of Hydrogen on the Corrosion of Steels in High-Temperature Water," *Corrosion 33(5),* pp. 173-178.

26. Sánchez-Moreno, M.; Takenoutib, H.; García-Jareñoc, J.J.; Vicentec, F.; Alonsoa, C. "A Theoretical Approach of Impedance Spectroscopy during the Passivation of Steel in Alkaline Media," *Electrochimica Acta, 54(28),* pp. 7222-7226.

27. Xu, W.; Daub, K.; Zhang, X.; Noel, J.J.; Shoesmith, D.W.; Wren, J.C. (2009). "Oxide Formation and Conversion on Carbon Steel in Mildly Basic Solutions," *Electrochimica Acta 54(24),* pp. 5727-5738.

28. Namduri, H.; Nasrazadani, S. (2008). "Quantitative Analysis of Iron Oxides Using Fourier Transform Infrared Spectrophotometry," *Corrosion Science 50(9),* pp. 2493-2497.

29. Kumai, C.S.; Devine, T.M. (2005). "Oxidation of Iron in 288°C Oxygen-Containing Water," *Corrosion 61(3),* pp. 201-218.

30. Tomlinson, L. (1981). "Mechanism of Corrosion of Carbon and Low-Alloy Ferritic Steels by High-Temperature Water," *Corrosion 37(10),* pp. 591-596.

31. Cheng, Y.; Steward, F. (2004). "Corrosion of Carbon Steels in High-Temperature Water Studied by Electrochemical Techniques," *Corrosion Science 46(10),* pp. 2405-2420.

32. Shibata, T.; Watanabe, M.; Taniguchi, N.; Shimizu, A. (September 2014). "Modelling of Carbon Steel Corrosion under an Oxygen-Depleted Environment," *Corrosion Engineering, Science and Technology 49(6),* pp. 435-441.

33. Bornak, W. (1988). "Chemistry of Iron and its Corrosion Products in Boiler Systems," *Corrosion 44(3),* pp. 154-158.

34. Joshi, P.; Venkateswaran, G.; Venkateswarlu, K. (1992). "Chelant Enhanced Passivation of Carbon Steel in Deoxygenated Alkaline Aqueous Solutions," *British Corrosion Journal 27(3),* pp. 200-206.

35. Joshi, P.; Venkateswaran, G.; Venkateswarlu, K. (1992). "Passivation Behavior of Carbon Steel Alloy in the Presence of EDTA, Ni (II) EDTA, and LiOH at 473°K," *Corrosion 48(6),* pp. 501-508.

36. Tvedt, T.; Wallace, S.; Griffin Jr., F. (1983). "Evaluation of On-Line Chelant Addition to PWR Steam Generators," steam generator cleaning project, Dow Chemical Co., Midland, MI.

37. Tvedt, T.; Wallace, S. (1987). "Chelant Passivation: New Study Challenges an Old Myth," *Power 131(2).*

38. Topp, H.; Hater, W.; Bache, A.B.; Kolk, C. (January 2012). "Film-Forming Amine in Shell Boilers," *PowerPlant Chemistry 14(1),* pp. 38-48.

39. Song, G.-D.; Jeon, S.-H.; Kim, J.-G.; Hur, D.-H. (August 2016). "Effect of Polyacrylic Acid on the Corrosion Behavior of Carbon Steel and Magnetite in Alkaline Aqueous Solutions," *Corrosion 72(8),* pp. 1010-1020.

40. Burleigh, T.D.; Dotson, T.C.; Dotson, K.T.; Gabay, J.; Sloan, T.B.; Ferrell, S.G. (January 2007). "Anodizing Steel in KOH and NaOH Solutions," *Journal of the Electrochemical Society 154(10),* pp. C579-C586.

41. Huijbregts, W.; Snel, A. (1972). "The Protection Effectiveness of Magnetite Layers in Relation to Boiler Corrosion": in 5th International Congress on Metallic Corrosion, Tokyo, Japan.

42. Dargahi, M.: Gaudreault, R.; Olsson, A.L.J.; Tufenkji, N. (Oct. 29-Nov. 1, 2014). "Green Chemistry: Purified Tannin Molecules for the Protection of Mild-Steel Closed-Loop Systems," technical paper presentation at the 2014 annual AWT Conference, Fort Worth, TX.

43. Dargahi, M.; Gaudreault, R.; Olsson, A.L.J.; Tufenkji, N. (November 2015). "Green Technology: Tannin-Based Corrosion Inhibitor for Protection of Mild Steel," *Corrosion 71(11),* pp. 1321-1329.

Endnote

A The tannin solutions used in the research came from TGWT Clean Technologies. Formulations used included TG 3106, TG 3124, and TG 3304.

Louis Godbout worked as a research assistant and academic associate at McGill University's Pulp and Paper Research Center for more than 20 years before joining TGWT Clean Technologies in 2016. He was one of the pioneers in the field of nanocrystalline cellulose research. Mr. Godbout developed several patents and published many articles on these materials as well as on the fundamental structure of the native cellulose crystal. Mr. Godbout has also been active in the field of scientific education. He is a volunteer on the STEM task force of the Association of Water Technologies. He can be reached at lgodbout@tgwt.com.

Axel Gambou-Bosca. Ph.D., is an R&D project manager at the Quebec Metallurgy Center, a technology transfer center affiliated to the "Cégep de Trois-Rivières." His work focuses on electrochemistry, corrosion, and surface science and touches on various industries. He is constantly working on providing knowledge, guidance, and solutions to mitigate in-service failure due to corrosion attack. Dr. Gambou-Bosca holds a Ph.D. in electrochemistry from the Université du Québec à Montréal. He may be reached at axel.gambou.bosca@cegeptr.qc.ca.
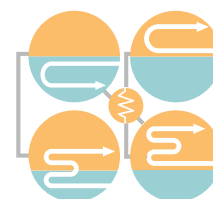
Christian Fowelin, Ph.D., is the head of R&D at Korn GmbH in Hamburg, Germany. He has more than 10 years of experience in the field of boiler water and cooling water treatment and dedicates his research to the further development of green chemistry aspects in industrial water applications. Dr. Fowelin studied chemistry at the University of Hamburg, where his research interests included metal organic complexes with ligands on the bases of modified naturally available amino sugars. He received his doctorate (Dr. rer. nat., summa cum laude) in 2009. Dr. Fowelin can be reached at cfowelin@tgwt.com.